Use of polar decomposition of Mueller matrices for optimizing the phase response of a liquid-crystal-on-silicon display

P. Clemente,[1] V. Durán,[2] Ll. Martínez-León,[2] V. Climent,[2] E. Tajahuerce,[2] and J. Lancis[2*]

[1] *Servei Central d'Instrumentació Científica, Universitat Jaume I, E12080 Castelló, Spain*
[2] *GROC·UJI, Departament de Física, Universitat Jaume I, E12080 Castelló, Spain*
[*] *Corresponding author: lancis@fca.uji.es*

Abstract: We provide experimental measurement of the Mueller matrices corresponding to an on-state liquid-crystal-on-silicon display as a function of the addressed voltage. The polar decomposition of the Mueller matrices determines the polarization properties of the device in terms of a diattenuation, a retardance and a depolarization effect. Although the diattenuation effect is shown to be negligible for the display, the behavior of the degree of polarization as a function of the input polarization state shows a maximum coupling of linearly polarized light into unpolarized light of about 10%. Concerning the retardation effect, we find that the display behaves as a retarder with a fast-axis orientation and a retardance angle that are voltage-dependent. The above decomposition provides a convenient framework to optimize the optical response of the display for achieving a phase-mostly modulation regime. To this end, the display is sandwiched between a polarization state generator and a polarization state analyzer. Laboratory results for a commercial panel show a phase modulation depth of 360º at 633 nm with a residual intensity variation lower than 6 %.

OCIS codes: (230.6120) Spatial light modulators; (230.3720) Liquid crystal devices; (120.5060) Phase modulation; (120.5410) Polarimetry.

References and links

1. D. J. McKnight, K. M. Johnson, and R. A. Serati, "256 x 256 Liquid-Crystal-on-Silicon Spatial Light-Modulator," Appl. Opt. **33**, 2775-2784 (1994).
2. H. T. Dai, K. X. Y. Liu, X. Wang, and J. H. Liu, "Characteristics of LCoS phase-only spatial light modulator and its applications," Opt. Commun. **238**, 269-276 (2005).
3. X. Wang, H. T. Dai, and K. Xu, "Tunable reflective lens array based on liquid cristal on silicon," Opt. Express **13**, 352-357 (2004).
4. Q. Mu, Z. Cao, L. Hu, D. Li, and L. Xuan, "Adaptive optics imaging system based on a high resolution liquid crystal on silicon device," Opt. Express **14**, 8013-8018 (2006).
5. S. T. Tang and H. S. Kwok, "3 x 3 Matrix for unitary optical systems," J. Opt. Soc. Am. A **18**, 2138-2145 (2001).
6. V. Duran, J. Lancis, E. Tajahuerce, and Z. Jaroszewicz, "Equivalent retarder-rotator approach to on-state twisted nematic liquid crystal displays," J. Appl. Phys. **99**, 113101-6 (2006).
7. S. Stallinga, "Equivalent retarder approach to reflective liquid crystal displays," J. Appl. Phys. **86**, 4756-4766 (1999).
8. S. T. Tang and H. S. Kwok, "Measurement of reflective liquid crystal displays," J. Appl. Phys. **91**, 8950-8954 (2002).
9. J. E. Wolfe and R. A. Chipman, "Polarimetric characterization of liquid-crystal-on-silicon panels," Appl. Opt. **45**, 1688-1703 (2006).
10. J. L. Pezzaniti and R. A. Chipman, "Mueller matrix imaging polarimeter", Opt. Eng. **34**, 1558-1568 (1995).
11. A. De Martino, Y. Kim, E. Garcia-Caurel, and B. Laude, "Optimized Mueller polarimeter with liquid crystals," Opt. Lett. **28**, 616-618 (2003).

#89833 - $15.00 USD Received 16 Nov 2007; revised 2 Jan 2008; accepted 2 Jan 2008; published 28 Jan 2008

12. S. Y. Lu and R. A. Chipman, "Interpretation of Mueller matrices based on polar decomposition," J. Opt. Soc. Am A **13**, 1106-1113 (1996).
13. J. M. Bueno, "Measurement of parameters of polarization in the living human eye using imaging polarimetry," Vis. Res. **40**, 3791-3799 (2000).
14. J. Chung, W. Jung, M. J. Hammer-Wilson, P. Wilder-Smith, and Z. Chen, "Use of polar decomposition for the diagnosis of oral precancer," Appl. Opt. **46**, 3038-3044 (2007).
15. J. L. Pezzaniti and R. A. Chipman, "Phase-only modulation of a twisted nematic liquid-crystal TV by use of the eigenpolarization states," Opt. Lett. **18**, 1567-1569 (1993).
16. J. A. Davis, I. Moreno, and T. Tsai, "Polarization eigenstates for twisted-nematic liquid-crystal displays," Appl. Opt. **37**, 937-945 (1998).
17. V. Duran, J. Lancis, E. Tajahuerce, and M. Fernandez-Alonso, "Phase-only modulation with a twisted nematic liquid crystal display by means of equi-azimuth polarization states," Opt. Express **14**, 5607-5616 (2006).
18. V. Duran, J. Lancis, E. Tajahuerce, and V. Climent, "Poincaré Sphere Method for Optimizing the Phase Modulation Response of a Twisted Nematic Liquid Crystal Display," J. Display Technol. **3**, 9-14 (2007).
19. D. Goldstein, *Polarized light* (Marcel Dekker, 2004).
20. S. R. Davis, R. J. Uberna, and R. A. Herke, "Retardance Sweep Polarimeter and Method," U. S. Patent, No. 6,744,509 (2004).
21. S. Y. Lu and R. A. Chipman, "Mueller matrices and the degree of polarization," Opt. Commun. **146**, 11-14 (1998).
22. R. M. A. Azzam and N. M. Bashara, *Ellipsometry and Polarized Light*, 1st edition, (Elsevier, Amsterdam, 1987).
23. K. H. Lu and B. E. A. Saleh, "Complex amplitude reflectance of the liquid-crystal light valve," Appl. Opt. **30**, 2354-2362 (1991).
24. A. Serrano-Heredia, G. W. Lu, P. Purwosumarto, and F. T. S. Yu, "Measurement of the phase modulation in liquid crystal television based on the fractional-Talbot effect," Opt. Eng. **35**, 2680-2684 (1996).
25. V. Duran, L. Martínez, Z. Jaroszewicz and A. Kołodziejczyk: "Calibration of spatial light modulators by inspection of their Fresnel images," European Optical Society, Topical Meetings Digest Series, **L-043**, (2005) (European Optical Society Topical Meeting on Diffractive Optics, 3 September - 7 September 2005, Warsaw, Poland).

1. Introduction

Commonly designed for high-resolution projection systems, liquid-crystal-on-silicon (LCoS) displays are programmable pixelated devices that operate in reflection. An LCoS pixel consists of a liquid crystal film over an aluminium electrode mirror controlled by a silicon integrated circuit [1]. LCoS displays are characterized by a high spatial resolution, with a pixel period that can be lower than 10 microns and a fill factor that can exceed the 90% [2]. Because of the above outstanding features, the use of LCoS displays as spatial light modulators (SLMs) in non-displays applications has gained considerable attention in recent years [2-4]. We consider a commercial LCoS panel with twisted nematic liquid crystal (TNLC) cells. From an optical point of view, a TNLC film is equivalent to a system composed of a linear retarder followed by a rotator [5-6]. For a reflective display, the rotation effect is cancelled by the double pass of the light through the medium. Therefore, a reflective TNLC display behaves in essence as a linear retarder with a neutral axis orientation and a retardance angle that are voltage-dependent [7]. This approach has been applied for optimizing the brightness and contrast of a reflective TNLC display [7], as well as for determining the design parameters of reflective TNLC cells [8].

Recently, Wolfe *et al*. have reported a complete polarimetric characterization of an LCoS panel showing a non-negligible depolarization effect [9]. As a result, the degree of polarization of the impinging light is reduced to a certain extent, which should be considered for proper operation. A depolarizing LCoS display working as intensity SLM can suffer from a severe diminution of the contrast ratio, leading to a worsening of the display performance. The physics of light depolarization has been attributed to electric field fluctuations and to edge effects in pixels or temperature variations. To deal with this effect, it is convenient to analyze light polarization devices in terms of Mueller matrices. Then, the state of polarization (SoP) is not described by the complex amplitudes of the electric field but by the corresponding Stokes vector. Experimental Mueller matrices of a LCoS cell have been measured with several

#89833 - $15.00 USD Received 16 Nov 2007; revised 2 Jan 2008; accepted 2 Jan 2008; published 28 Jan 2008

polarimetric techniques [10,11]. Between them, it should be mentioned those based on nematic liquid crystal variable retarders [11]. From an optical point of view, the diattenuation, the retardance and the depolarization of the input polarized light fully characterizes the behavior of the LCoS cells. The above effects can be conveniently separated by the so-called polar decomposition of the Mueller matrix introduced by Lu and Chipmann [12]. Here, the action of any polarization device is decomposed as the association of a pure diattenuattor, a pure retarder, and a pure depolarizer. The polar decomposition, especially when used for polarimetric imaging, has proved to be a powerful tool for studying the polarization properties of a sample in a widespread set of applications [13,14].

In the framework of non-display applications of SLMs, a precise spatial control of the phase of an input wavefront is required. Usually, TNLC displays operating in transmission have been employed for wavefront phase-only modulation [15-18]. The display is inserted in a polarimetric arrangement that includes a polarization state generator (PSG) and a polarization state analyzer (PSA). The above devices consist of a linear polarizer and a quarter-wave plate. The output light intensity must be constant in the optimal configuration of the polarimetric arrangement. Some attempts have been done in order to achieve a phase-mostly modulation of the wavefront by use of a LCoS display [2]. This is a major challenge due to the outstanding features of LCoS displays concerning spatial resolution and fill factor. The phase modulation provided by the display is due, on the one hand, to the well-known voltage-controllable birefringence of the medium and, on the other hand, to the effect of the equivalent pure retarder [17]. Again, the display is inserted between a PSG and a PSA. Up to now, the search for the optimal configuration has been performed by means of the Jones calculus as diattenuation and depolarization effects have not been incorporated. However, as noted by Wolfe [9], depolarization effect plays a significant role in the behavior of an LCoS display.

In this paper, we perform, for the first time to our knowledge, the full characterization of an LCoS display, including light depolarization, for phase-mostly modulation of the wavefront. To this end, the behavior of the whole optical setup is performed by use of the Mueller-Stokes algebra. Although in principle this is a major drawback for phase-only modulation applications, as the information about the phase of the totally polarized light component emerging from the whole device is discarded, we show how the polar decomposition of the Mueller matrix provides a convenient framework. To this end, we extract the retardance parameters of the LCoS display. Therefore, combining both Jones and Stokes formalisms, the configuration of the PSG and the PSA is optimized for achieving a phase-only modulation regime. In Sec. 2, and for the sake of completeness, we review the theory of polar decomposition, defining the relevant polarization parameters. In Sec 3, we describe the laboratory set-up for measuring the Mueller matrix of the LCoS as a function of the voltage. In Sec. 4, we present the calculations, based on the polar decomposition, for optimizing the phase response of the LCoS display and show the experimental operating curve for the LCoS display. Conclusions are summarized in Sec. 5.

2. Theory of polar decomposition

Three-factor polar decomposition of the Mueller matrix **M**, firstly proposed by Lu and Chipman, allows one to decompose the action of any polarizing device as the product of three elementary devices; a pure diattenuator, $\mathbf{M}_D$, a pure retarder, $\mathbf{M}_R$, and a pure depolarizer, $\mathbf{M}_\Delta$ [12]. In mathematical terms,

$$\mathbf{M} = \mathbf{M}_\Delta \mathbf{M}_R \mathbf{M}_D . \tag{1}$$

Note that the order in which the matrices are multiplied is a relevant feature. The intensity reflected by an LCoS display has been shown to be independent of the input polarization state [9]. In other words, for an LCoS cell diattenuation is a minor effect that can be neglected to provide a simplified Mueller matrix $\mathbf{M}_{LCoS}$

$$\mathbf{M}_{LCoS} = \mathbf{M}_\Delta \mathbf{M}_R \ . \tag{2}$$

#89833 - $15.00 USD Received 16 Nov 2007; revised 2 Jan 2008; accepted 2 Jan 2008; published 28 Jan 2008

It is well-known that the action of a pure retarder on the input polarized light can be geometrically described over the surface of the Poincaré sphere by means of a rotation along the fast axis of the device [19]. Thus, $\mathbf{M}_R$ results

$$\mathbf{M}_R = \begin{bmatrix} 1 & \vec{0}^T \\ \vec{0} & \mathbf{m}_R \end{bmatrix}, \tag{3}$$

where $\vec{0}$ is the three-element zero vector and $\mathbf{m}_R$ is the three-dimensional rotation matrix,

$$(\mathbf{m}_R)_{ij} = \delta_{ij}\cos R + a_i a_j (1-\cos R) + \sum_{k=1}^{3} \varepsilon_{ijk} a_k \sin R, \quad i, j = 1,2,3\,. \tag{4}$$

In Eq. (4), δ_{ij} is the Kronecker delta, ε_{ijk} is the Levi-Cevità tensor, R is the retardance angle, and $(1, a_1, a_2\, a_3)^T$ is the normalized Stokes vector corresponding to the eigenstate along the fast axis of the retarder. Inversely, R and the components a_i, i=1,2,3, are obtained from $\mathbf{M}_R$ as

$$R = \begin{cases} \cos^{-1}\left[\dfrac{tr(\mathbf{M}_R)}{2} - 1\right] & 0 \le R \le \pi \\ 2\pi - \cos^{-1}\left[\dfrac{tr(\mathbf{M}_R)}{2} - 1\right] & \pi \le R \le 2\pi \end{cases}, \tag{5}$$

and

$$a_i = \frac{1}{2\sin R} \sum_{j,k=1}^{3} \varepsilon_{ijk} (\mathbf{m}_R)_{jk}\,. \tag{6}$$

with $tr(\mathbf{M}_R)$ the trace of the retarder matrix. Finally we account for the coupling of polarized light into unpolarized light through the depolarization matrix $\mathbf{M}_\Delta$

$$\mathbf{M}_\Delta = \begin{bmatrix} 1 & \vec{0}^T \\ P_\Delta & \mathbf{m}_\Delta \end{bmatrix}, \tag{7}$$

where $\mathbf{m}_\Delta$ is a 3×3 symmetric matrix, $\mathbf{m}_\Delta^T = \mathbf{m}_\Delta$, and P_Δ is the so-called polarizance vector, which, in the absence of diattenuattion, is given by the first column of $\mathbf{M}_{LCoS}$. On the other hand, the averaged depolarization capability of the equivalent depolarizer, the so-called depolarization power Δ, is then given by

$$\Delta = 1 - \frac{\left|tr(\mathbf{m}_\Delta)\right|}{3}, \quad 0 \le \Delta \le 1\,. \tag{8}$$

Now we focus on the extraction of the $\mathbf{m}_\Delta$ and $\mathbf{m}_R$ matrices from the experimental Mueller matrix of an LCoS display $\mathbf{M}_{LCoS}$. To this end, we begin by recognizing that, by taking into account Eqs. (3) and (7), Eq. (2) can be rewritten as

$$\mathbf{M}_{LCoS} = \begin{bmatrix} 1 & \vec{0}^T \\ P_\Delta & \mathbf{m}_\Delta \mathbf{m}_R \end{bmatrix} = \begin{bmatrix} 1 & \vec{0}^T \\ P_\Delta & \mathbf{m}' \end{bmatrix}, \tag{9}$$

where $\mathbf{m}' \equiv \mathbf{m}_\Delta \mathbf{m}_R$. Taking into account that $\mathbf{m}_\Delta$ is a symmetric matrix, it is straightforward to show that $\mathbf{m}_\Delta{}^2 = \mathbf{m}'(\mathbf{m}')^T$. To extract the depolarization matrix we follow the Cayley-Hamilton theorem. In this way,

$$\begin{aligned} \mathbf{m}_\Delta = \pm\Big[\mathbf{m}'(\mathbf{m}')^T + (\sqrt{\lambda_1}\lambda_2 + \sqrt{\lambda_2}\lambda_3 + \sqrt{\lambda_3}\lambda_1)\mathbf{I}\Big]^{-1} \\ \times\Big[(\sqrt{\lambda_1} + \sqrt{\lambda_2} + \sqrt{\lambda_3})\,\mathbf{m}'(\mathbf{m}')^T + \sqrt{\lambda_1\lambda_2\lambda_3}\,\mathbf{I}\Big] \end{aligned}, \tag{10}$$

#89833 - $15.00 USD Received 16 Nov 2007; revised 2 Jan 2008; accepted 2 Jan 2008; published 28 Jan 2008

where λ_1, λ_2, and λ_3 are the eigenvalues of $\mathbf{m}'(\mathbf{m}')^T$ and $\mathbf{I}$ is the 3×3 identity matrix. The sign in the right-hand side of Eq. (10) follows the sign of the determinant of $\mathbf{m}'$. With the above expression for $\mathbf{m}_\Delta$, $\mathbf{M}_\Delta$ can be determined through Eq. (7) and $\mathbf{M}_R$ can be obtained by

$$\mathbf{M}_R = \mathbf{M}_\Delta^{-1}\mathbf{M}_{LCoS} . \quad (11)$$

3. Mueller matrix measurement

3.1. Experimental set-up

The laboratory set-up for the determination of the the matrix elements $M_{\alpha\beta}$, α, β = 0,1,2,3, of the LCoS display is shown in Fig. 1. The radiation coming from a He-Ne laser (LS) emitting at 633 nm is spatially filtered and collimated by the lens L_1 to provide a homogeneous beam with a diameter of 15 mm. The LCoS display is an Aurora panel, with XGA resolution (1024×768 pixels) and a size of 19.6×14.6 mm, commercialized by Holoeye. The TNLC cells have a twist angle of 45º and the pixel array has a period of 19 μm with an inactive gap of 1μm. The voltage is applied to the pixels by displaying an image codified into a 2^8 gray-level scale. For our display, the voltage increases monotonically with the gray level. The radiation impinges onto the LCoS cells at a quasi-normal incidence ($\alpha = 4^o$) so that the input and the reflected beams are spatially separated and the Stokes formalism can be applied. Note that as a result of the pixelated structure of the display, the outgoing energy splits into several diffraction orders. The zero order was isolated for all intensity measurements. We used a PSG to generate the different SoPs required to measure the Mueller matrix of the display. The PSG comprises a linear polarizer P_1 followed by a zero-order quarter-wave plate QWP at 633 nm. On the other hand, the PSA is a home-built Stokesmeter constituted by two nematic liquid crystal variable retarders ($LCVR_1$ and $LCVR_2$), a linear polarizer P_2. A focusing lens L_2 is used to focus the light into the photometer PM. The LCRV retardance is controlled by the application of a voltage. The Stokes vector is extracted from the least-square fitting of the intensity data collected at the photometer as the retardance value of each LCRV is

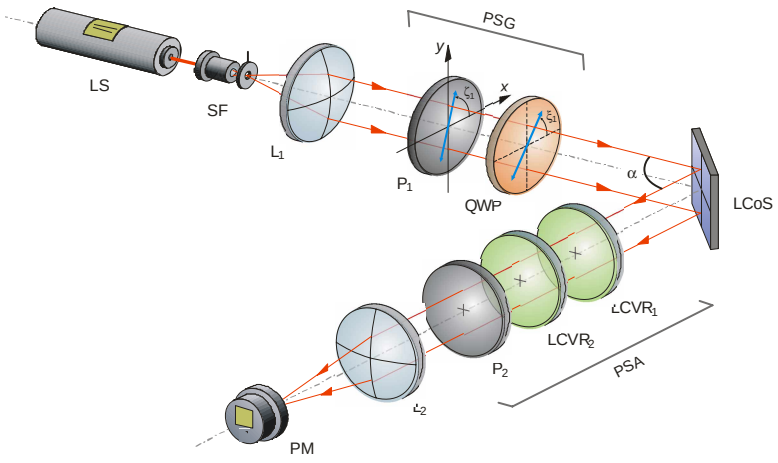

Fig. 1. Experimental set-up for measuring the LCoS Mueller matrices.

sequentially changed by application of a voltage sweep [20]. A set of twenty-five intensity measurements allows us to achieve a maximum uncertainty for the Stokes parameters of 0.03. Provided that the PSG is composed of non-ideal optical elements, we used our Stokesmeter to

#89833 - $15.00 USD Received 16 Nov 2007; revised 2 Jan 2008; accepted 2 Jan 2008; published 28 Jan 2008

measure the actual polarization states of the light impinging onto the liquid crystal cells to increase the precision of the experiment.

The first row of the Mueller matrix is obtained without the use of the PSA, as only reflectance measurements should be made. We normalized the measurements by using the LCoS reflectance for unpolarized input, so that M_{00}=1 for any addressed gray level. Concerning the matrix elements in the first row, M_{01} is obtained as the difference between the normalized reflectance values for linearly polarized input light in the horizontal and the vertical direction. Analogously, M_{02} and M_{03} result, respectively, from the differences for linearly polarized input light at 45º and 135º, and for right and left circularly polarized light. Note that, as M_{00}=1, the matrix elements M_{0i} (i = 1, 2, 3) coincide with the diattenuation coefficients D_{H}, D_{45} and D_{C}, respectively [19]. In our measurements, we found that all of these coefficients are always less than 0.016 in absolute value, with a mean value along the entire gray level range below 0.008. In addition to the diattenuation coefficients, a generally accepted indicator for characterizing the degree of diattenuation of an optical component is the polarization dependent loss (PDL). This parameter is defined as PDL = 10 log (R_{max}/R_{min}), where R_{max} and R_{min} correspond, respectively, to the maximum and minimum reflectance values, which can be calculated for any gray-level from the first row of the Mueller matrix [12]. For our LCoS display, the mean value of PDL is 0.12 dB. As in Ref [9], we conclude that the diattenuation effect is negligible.

The rest of the the Mueller matrix elements were measured with the whole arrangement in Fig. 1. To this end, we generated four different SoPs, represented by the Stokes vectors $\mathbf{S}_i$ (i = 1,...,4), corresponding to horizontal, vertical and 45º linearly polarized light, and right-handed circularly polarized light, respectively. We constructed a 4×4 matrix $\mathbf{N}_1$, whose columns are the input vectors $\mathbf{S}_i$. Afterwards, the Stokes parameters for each light emerging from the display $\mathbf{S}_i'(g)$ were measured. For each value of the gray level, these vectors, arranged in columns, determine a second 4×4 matrix $\mathbf{N}_2$ (g). The matrices $\mathbf{N}_1$ and $\mathbf{N}_2$(g) are related through the equation $\mathbf{N}_2(\mathrm{g}) = \mathbf{M}_{LCoS}(\mathrm{g})\ \mathbf{N}_1$. Therefore, the Mueller matrices $\mathbf{M}_{LCoS}(g)$ were obtained as $\mathbf{M}_{LCoS}(g) = \mathbf{N}_2(g)\ \mathbf{N}_1^{-1}$. In our experiment, the gray level value was changed in steps of 8.

3.2. Depolarization effect

Once the LCoS Mueller matrices were determined, we applied the polar decomposition given by Eq. (2). Experimental $\mathbf{M}_{LCoS}(g)$ matrices show the structure in Eq. (8) with a nule polarizance vector, P_Δ(g). From the 3×3 submatrix $\mathbf{m}'$, the depolarization Mueller matrices $\mathbf{M}_\Delta(g)$ were obtained through Eqs. (7) and (10). Figure 2(a) shows the experimental values for the depolarization power, $\Delta(g)$, calculated in accordance with Eq. (8). This parameter shows a maximum value of about 5% along the entire pixel dynamic range. Thus, the depolarization effect due to the LCoS can not be neglected. From a practical point of view, the coupling of polarized light into unpolarized light depends on the input SoP so that the depolarization power only provides a rough estimate. This dependence is observed in the degree of polarization (*DoP*) which is defined from the Stokes parameters S_i (i = 0,...,3) as [19]

$$DoP = \frac{\sqrt{S_1^2 + S_2^2 + S_3^2}}{S_0}. \qquad (12)$$

#89833 - $15.00 USD Received 16 Nov 2007; revised 2 Jan 2008; accepted 2 Jan 2008; published 28 Jan 2008

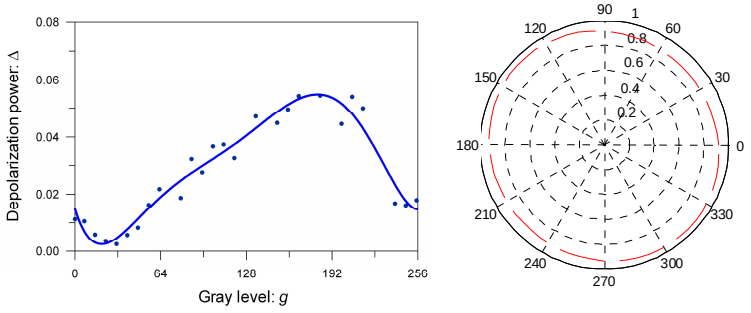

(a) (b)

Fig. 2. (a). Depolarization power provided by the LCoS display for a wavelength of 633 nm and (b) deformation of the Poincaré sphere equator due to the LCoS display for g=200.

This parameter takes values between 1 (totally polarized light) and 0 (unpolarized light). Geometrically, the *DoP* is given by the distance between the origin and the point in the Stokes-parameter space associated to the SoPs. Points over the surface of the Poincaré sphere represent polarized light whereas interior points correspond to partially polarized light. It is well-known that a pure depolarizer transforms the set of SoPs over the Poincaré sphere into an ellipsoid [21]. We carried out a preliminary verification by impinging the LCoS with linearly polarized input light. We chose g=200. Results are shown in Fig. 2(b). Here, the shrinkage of the equatorial circle of the Poincaré sphere is clearly noticeable. The *DoP* reaches a maximum value of approximately 10% for input azimuths around 22.5º and 112.5º (recall that azimuths are doubled in the Poincaré sphere representation). Note that the azimuth of the input linearly polarized light corresponding to the maximum depolarization effect depends on the orientation of the depolarization ellipsoid, which, in general, changes with the gray-level g.

3.3. Retardance effect

Finally, the retardance matrices $\mathbf{M}_R(g)$ were obtained through Eq. (11). From the above set of data, the retardance angle $R(g)$ and the azimuth and the ellipticity angles corresponding to the fast axis orientation, $\theta(g)$ and $\varepsilon(g)$, were calculated in accordance with Eqs. (5) and (6), respectively. Note that for each gray level $\theta = (1/2)\arctan(a_2/a_1)$ and $\varepsilon = (1/2)\arcsin(a_3)$ [19]. Results are shown in Fig. 3. For $g = 0$ the fast axis is oriented along the vertical direction while for g=255 the azimuth θ is close to −45º and the equivalent retarder behaves approximately as a half-wave plate. These facts suggest the underlying mechanisms of the behavior of the LCoS display as an intensity modulator. It also should be noted that the magnitude of the ellipticity angle $\varepsilon(g)$ raises along the gray level range, which points out that the fast axis becomes slightly located outside the equator of the Poincaré sphere. In other words, the retardance properties of the LCoS display for high values of the gray level are best fitted by an elliptic retarder [21]. Although, in principle, a reflective LCoS cell acts as a linear retarder by the double pass of the light through the liquid crystal [7], some deviations are originated by small alterations of the SoP during the reflection inside the pixel.

4. Optimization of the LCoS phase modulation response

After the display characterization performed in Section 3, we optimize the phase response of the LCoS. To this end, the LCoS is inserted in between a PSG constituted by a linear polarizer followed by a zero-order quarter-wave plate at 633 nm and a PSA consisting of identical elements but in reversed order. Concerning the PSG, the transmission axis of the linear polarizer and the fast axis of the quarter wave plate are oriented at angles ζ_1 and ξ_1 from the

#89833 - $15.00 USD Received 16 Nov 2007; revised 2 Jan 2008; accepted 2 Jan 2008; published 28 Jan 2008

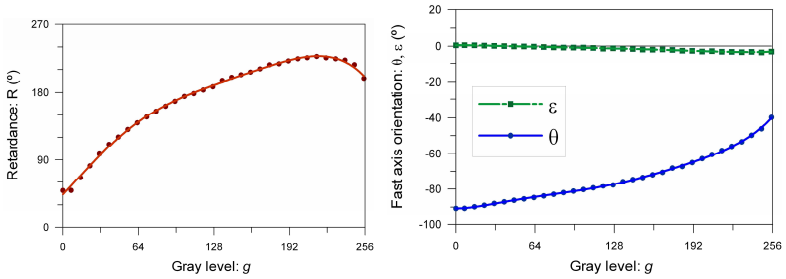

(a) (b)

Fig. 3. (a). Retardation angle and (b) orientation of the retarder fast axis for a wavelength of 633.

horizontal direction in the laboratory framework, respectively. Analogous angles are denoted by ζ_2 and ξ_2 for the PSA. The Stokes vector **S'** corresponding to the light emerging from the last polarizer is given by

$$\mathbf{S'}(g,\zeta_1,\xi_1,\zeta_2,\xi_2\ ) = \mathbf{M}_P(\zeta_2)\mathbf{M}_{QWP}(\xi_2)\mathbf{M}_{LCoS}(g)\mathbf{M}_{QWP}(\xi_1)\mathbf{S}(\zeta_1), \tag{13}$$

where $\mathbf{S} = (1, \cos 2\zeta_1, \sin 2\zeta_1, 0)^T$ and $\mathbf{M}_P$ and $\mathbf{M}_{QWP}$ are, respectively, the conventional Mueller matrices for a linear polarizer and a quarter wave plate [19],[22].

The intensity response of the above arrangement is evaluated for any angular configuration of the PSG and the PSA by means of $S_0'(g)$. It is worth mentioning that no information about the phase of the outgoing light is obtained using the Mueller matrix formalism. However, for some applications, it is also important to evaluate the phase modulation of the totally polarized light component emerging from the LCoS display. This task can be accomplished by use of the Jones calculus as we will show next.

We begin by describing the SoP of an arbitrary totally polarized light beam through the complex variable χ as

$$\chi = \frac{\tan\theta + j\tan\varepsilon}{1 - j\tan\theta\tan\varepsilon}, \tag{14}$$

where θ and ε are, respectively, the azimuth and the ellipticity angle of the polarization ellipse, and j is the imaginary unit. This characterization was first introduced by Poincaré and later developed by Azzam and Bashara [22]. Within this framework, the Jones matrix for an elliptic retarder with a retardance angle R and a fast eigenstate described by χ_{ef} is [22]

$$\mathbf{J} = \left(1 + \chi_{ef}\,\chi_{ef}^{*}\right)^{-1} \times \begin{pmatrix} \exp(jR/2) + \chi_{ef}\,\chi_{ef}^{*}\exp(-jR/2) & 2j\chi_{ef}^{*}\sin(R/2) \\ 2j\chi_{ef}\sin(R/2) & \exp(-jR/2) + \chi_{ef}\,\chi_{ef}^{*}\exp(jR/2) \end{pmatrix}. \tag{15}$$

Here the symbol * denotes the complex conjugate. Note that **J** is a unitary matrix. By using the values for $\theta(g)$, $\varepsilon(g)$, and $R(g)$ in Fig. 3, we obtain the Jones matrices $\mathbf{J}_{LCoS}(g)$ as a function of the gray level. The real and imaginary parts of J_{11} and J_{12} are represented in Fig. 4. Next, the components of the electric field at the output of the PSG-LCoS-PSA system are

$$\begin{pmatrix} E_x \\ E_y \end{pmatrix} = \exp(-j2\beta)\,\mathbf{J}_P(\zeta_2)\mathbf{J}_{QWP}(\xi_2)\mathbf{J}_{LCoS}\,\mathbf{J}_{QWP}(\xi_1)\begin{pmatrix} \cos\zeta_1 \\ \sin\zeta_1 \end{pmatrix}. \tag{16}$$

Here $\mathbf{J}_P$ and $\mathbf{J}_{QWP}$ correspond to the conventional Jones matrices of a polarizer and a quarter wave plate, respectively (see Ref. [19] and [22]). The angle β is the birefringence parameter

#89833 - $15.00 USD Received 16 Nov 2007; revised 2 Jan 2008; accepted 2 Jan 2008; published 28 Jan 2008

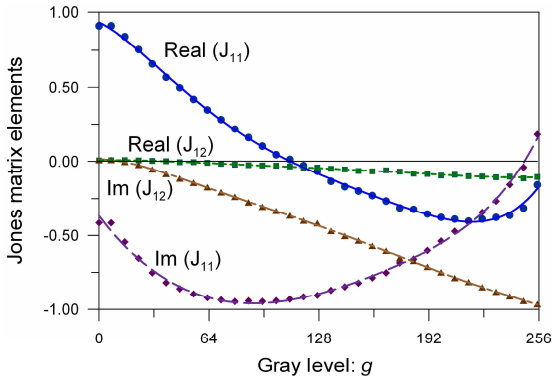

Fig. 4. Jones matrix elements corresponding to the retardance effect of the LCoS display

defined as $\beta=\pi\, d\Delta n\, /\lambda$, where d is the cell thickness, Δn is the difference between the extraordinary and the ordinary refraction index, and λ is the wavelength. Four our display, d = 5.5 μm and Δn~0.1 in the off-state [3]. Note the effect originated by the double pass of the light through the medium [23]. Of course, the Jones vector in Eq. (16) corresponds to a light beam polarized in the direction of the transmission axis of the last analyzer. More conveniently, this vector can be written in the analyzer framework as

$$\begin{pmatrix} E_x \\ E_y \end{pmatrix} = \exp(-j2\beta)\begin{pmatrix} a+jb \\ 0 \end{pmatrix}, \tag{17}$$

where a and b are quantities that depend on the gray level g and on the angular configurations of the PSG and PSA. From the above equation the total phase shift φ introduced by the polarization arrangement is given by

$$\varphi(g,\zeta_1,\xi_1,\zeta_2,\xi_2) = -2\beta(g) + \arctan\left[\frac{b(g,\zeta_1,\xi_1,\zeta_2,\xi_2)}{a(g,\zeta_1,\xi_1,\zeta_2,\xi_2)}\right]. \tag{18}$$

It is important to note that the birefringence parameter $\beta(g)$ is a decreasing function of the applied voltage [23], i.e., a decreasing function of the gray-level for our display.

Now, let us recover the phase-mostly modulation question. We look for the optimal angular configurations of the PSG and PSA satisfying: 1) a minimum variation for the transmitted intensity $S_0'(g)$; and 2) a maximum variation of the phase shift $\varphi(g)$. Here, we also demand that an increasing behavior with the gray level for the term depending on the quantities a and b just to add constructively with the birefringence term $-2\beta(g)$. Note both the Stokes and the Jones calculus are employed in our determination. Taking into account the values previously determined for $\mathbf{M}_{LCoS}$ and χ_{ef}, we perform the numerical computation of $S_0'(g,\zeta_1,\xi_1,\zeta_2,\xi_2)$ and $\varphi(g,\zeta_1,\xi_1,\zeta_2,\xi_2)$, using Eqs. (13) and (18), respectively. The full range of values for the angular variables ζ_1,ξ_1,ζ_2, and ξ_2 was covered in steps of 1º. In this way, we found the optimal angular configuration of our system when ζ_1=94º, ξ_1=163º, ξ_2=179º, and ζ_2=99º. With this set of angular variables the mean value for $S_0'(g)$ is about 62% with a residual variation lower than 3%.

Finally we experimentally test the whole LCoS response. To this end, we construct the operation curve of the display, where the complex amplitude response is drawn in a polar plot as a function of the addressed gray level. The curve was constructed by experimental measurement of the transmitted intensity and the phase introduced by the LCoS. To measure the phase, we used a technique based on the fractional Talbot effect [17], [24,25]. In short, we

#89833 - $15.00 USD Received 16 Nov 2007; revised 2 Jan 2008; accepted 2 Jan 2008; published 28 Jan 2008

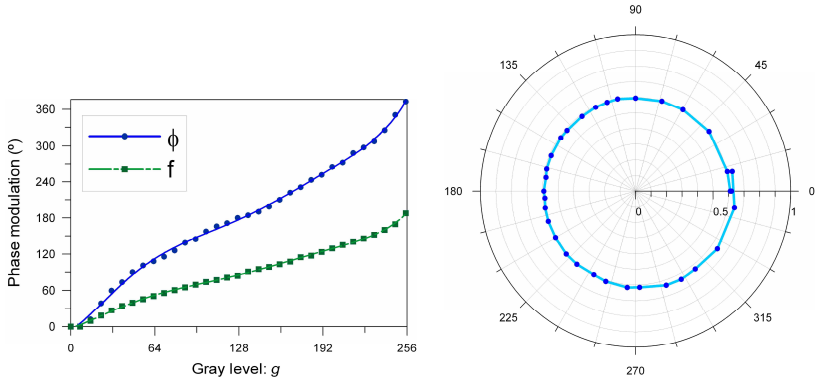

(a) (b)

Fig. 5. Modulation provided by the LCoS display in the phase-mostly configuration. a) Phase shift versus gray level and b) operation curve.

imprint onto the LCoS display a pattern consisting of a binary diffraction grating; one gray level is fixed to g=0 whereas the other ranges along the entire pixel dynamic range. The relative phase shift $\Delta\varphi=\varphi(g)-\varphi(0)$ is determined by measuring the contrast of the Fresnel images at a quarter of the Talbot distance of the periodic pattern. Concerning the transmitted intensity $S_0'(g)$, it was measured with a photometer by displaying onto the LCoS a uniform image. Fig. 5(a) shows a plot of the phase-shift $\Delta\varphi$ versus the gray level g in the phase-mostly configuration. We have also represented the function $f(g)$= arctan[$b(g)/a(g)$]–arctan[$b(0)/a(0)$] calculated from Eq. (16). The difference between $\Delta\varphi$(g) and $f(g)$ gives the variation along the gray level range of the birefringence term that appears in Eq. (18). Finally, Fig. 5(b) shows the LCoS operation curve. The radius and polar angle of each point of this curve represent, respectively, the transmitted intensity and the phase shift for a given value of the addressed gray level. The experimental results are close to a pure phase modulation regime. Further, maximum phase-modulation depth greater than 360º is achieved.

5. Conclusions

We have achieved phase-mostly modulation of the wavefront by means of an LCoS display. To this end, we have inserted the display into a polarimetric arrangement consisting of a polarization state generator and a polarization state analyzer constituted by a polarizer and a zero order quarter-wave plate. Previously the LCoS was calibrated following the polar decomposition of the Mueller matrix. Although the diattenuation effect was shown to be negligible, the effect of light depolarization must be taken into account for proper operation of the cells. A depolarization effect as high as 10% was measured for certain states of polarization of the input light. Finally, the analysis of the retardance behaviour is performed within the conventional Jones formalism. Our technique allows one to optimize the angular configuration of the polarimetric arrangement to achieve a flat intensity response (a residual error lower than 6%) with a broad phase response (as high as 360º). Experimental measurements in the laboratory corroborate the optimization algorithm. This technique benefits from the high spatial resolution and excellent fill factor of commercial panels made on silicon.

Acknowledgments

This research was funded by the Conveni Fundació Caixa Castelló-Bancaixa-Universitat Jaume I, Spain, under the project P1 1B2006-29. We also acknowledge financial support from the Ministerio de Educación y Ciencia and FEDER under the project FIS2007-62217.

#89833 - $15.00 USD Received 16 Nov 2007; revised 2 Jan 2008; accepted 2 Jan 2008; published 28 Jan 2008